AIAA JOURNAL
Vol. 37, No. 5, May 1999

Static Shape Control of Smart Structures Using Compliant Mechanisms

Laxminarayana Saggere* and Sridhar Kota†
University of Michigan, Ann Arbor, Michigan 48109

A novel approach to static shape control of smart structures is introduced. This approach uses a special class of mechanisms called compliant mechanisms powered by a single input actuator. The key design issue in this approach is the synthesis of a suitable compliant mechanism for the task. A systematic procedure for synthesis of such compliant mechanisms is presented by combining the first principles of mechanics and kinematics through a structural optimization scheme. The procedure is illustrated by an example wherein a prescribed smooth shape change in the camber of an idealized airfoil structure is accomplished by a specially synthesized compliant mechanism actuated by a single torque input. The scope and benefits of the proposed approach in providing viable simple solutions for real-scale static shape control applications are also discussed.

Introduction

A SMART structure is defined as "a non-biological physical structure having a definite purpose, means and imperative to achieve that purpose, and a biological pattern of functioning."[1] Smart structures are employed in a variety of applications, mostly control of vibration and shape in several fields, especially space, aircraft, and automotive engineering. Shape control is an important task of smart structures and, in general, it means control of position or alignment of a certain number of points on the structure so as to track a desired value. In large space systems such as antenna reflectors, shape control generally is employed to maintain the precise shape of a structure by effecting high-precision corrections to any deviations from the primary configuration of the structure.[2,3] In other systems such as aircraft wing structures, shape control is employed to adaptively effect controlled, finite deformations in a flexible structure in response to changes in the operational conditions of the structure.[4,5] The new approach presented here concerns the latter type of shape control, viz. effectuation of controlled finite deformations in a flexible structure. Some important issues in such a type of shape control are examined in the following through a brief discussion of adaptive camber shaping of aircraft wings.

The concept of adaptive variable camber wing (VCW) has been studied extensively to improve significantly the aerodynamic performance of an aircraft in flight.[6–12] VCW is implemented in modern transport aircraft, e.g., Airbus A340 and Boeing 757, (Refs. 13 and 14) and has been tested on combat aircraft, e.g., Mission Adaptive Wing (MAW),[15] by means of traditional high-lift devices actuated by conventional mechanical schemes. However, the VCW schemes implemented in transport aircraft involve discontinuities or sudden curvature changes in the airfoil cross section resulting in early flow separation and limitation of the maximum achievable optimal lift/drag ratios. The VCW scheme tested in MAW eliminated the discontinuities by enclosing the control surfaces within a smooth flexible skin, but the scheme involved an actuation system that was rather complex and bulky.[16] Recent advent of highly compact actuators using smart materials has provided the scope for accomplishing a smooth VCW without considerable weight penalties. Using this smart materials technology, researchers have studied several innovative schemes[17–22] to vary the wing camber. The general idea behind these schemes is to induce strain in the structure by interfacing it with smart materials, particularly piezoelectrics and shape memory alloys (SMAs), as either a few discrete actuators at the macroscopic level or a distributed network of actuators at the mesoscopic level. The experimental tests conducted on scaled models to qualify the smart materials for static shape control of wing structures in these studies[17–22] indicate that, although smart materials-based technology holds promise for shape control of aircraft wings, its transition to real-scale models is impeded by the limitations of the present-day smart materials. The most serious limitation of currently available smart materials is their feeble stroke and power, and this seems to be placing a practical limitation on the achievable induced strain levels without encumbering the weight of the system. Currently, piezoelectric actuators have high bandwidth but low strain, whereas SMA actuators have relatively higher strain but extremely low bandwidth. Therefore, use of smart materials for strain actuation involves strain vs weight vs bandwidth tradeoff.[23] Moreover, the involvement of a rather large number of actuators in the smart materials-based schemes directly impacts the complexity of the control system.

We present a new scheme to accomplish static shape control of smart structures without the drawbacks of the conventional mechanical schemes or the smart materials-based schemes. This scheme is capable of accomplishing prescribed small shape changes in flexible beam segments within certain prescribed tolerance of error using only a single input actuator (not restricted to smart materials). The proposed scheme does not involve rigid links and hinge joints as in conventional mechanisms, and it is not prone to shortcomings such as inadequacy of actuation power, excessive weight, and complexity for real-scale applications. Basically, in this approach the required shape deformation of a given structure is achieved by transmitting controlled displacements and energy from an actuator installed at a convenient location away from the deforming structure through a special class of mechanisms called compliant mechanisms. A brief description of compliant mechanisms is provided before the details of the new approach are presented.

Compliant Mechanisms

Compliant mechanisms are a class of mechanisms that achieve mobility, at least in part, though flexure, i.e., elastic deformation of one more of their constituent segments, rather than exclusively through relative motion at the joints as in the case of the traditional rigid-link mechanisms.[24] Apparently, a compliant mechanism comprises link(s) and/or joint(s) that are flexible, unlike a traditional mechanism whose links and joints are all designed to be rigid. Compliant mechanisms have several functional advantages (they are lighter weight and generate a variety of precision motions free of backlash, friction, and noise) and economical advantages (they require no assembly and can be batch produced). Owing to these advantages, compliant mechanisms are increasingly finding

Received March 16, 1998; revision received Dec. 9, 1998; accepted for publication Dec. 15, 1998.

*Graduate Student Research Assistant, Department of Mechanical Engineering and Applied Mechanics; currently Research Fellow, Department of Mechanical Engineering and Applied Mechanics. Member AIAA.

†Associate Professor, Department of Mechanical Engineering and Applied Mechanics.

a variety of applications ranging from scores of simple products such as pliers and staplers[25] used in everyday life to sophisticated precision instruments[26] and microelectromechanical systems (MEMS).[27,28]

A compliant mechanism can be either monolithic or nonmonolithic in construction. In a monolithic compliant mechanism, the flexure action could be either highly localized at discrete locations, as in flexural pivots obtained by "necking" down a small region of a thick blank of material, or be more or less continuously distributed in all segments of the mechanism. Based on this criterion, compliant mechanisms are classified as lumped and distributed, respectively. Although flexural pivots have been in wide practical use since the early part of this century,[29] compliant mechanisms have been studied systematically as a special class of mechanisms only in the past three decades beginning with the academic research conducted by Burns.[30] Since then, researchers have proposed a few methods for synthesis of various types of compliant mechanisms for various objectives.[31–34] We introduce a new method for synthesis of distributed-type compliant mechanisms to accomplish a novel objective, viz. effectuating prescribed shape changes in a given beam segment.

New Approach

Consider that a smoothly curved slender beam segment with known initial shape, elastic properties, boundary conditions, and external loading, if any, is required to be shaped into a specified definite smooth shape. Effectuation of such a continuous shape change in a beam generally requires a continuously distributed load (bending moment) along the length of the member according to Euler's elastic curve equation. However, to circumvent the complications associated with generating a continuously distributed load on the beam segment by means of embedded actuation, the new approach incorporates a tradeoff. That is, in lieu of the exact desired shape change, a very close approximation is accomplished by activating the given beam segment at a few discrete points using energy from a single input actuator removed from the beam segment. This transfer of energy is effected through a single-input/multi-output compliant mechanism. That is, a compliant mechanism is connected at its input end to an actuation source (torque or rotation), and its output ends are connected to the given beam segment at a finite optimal number of discrete points. The compliant mechanism stores the input energy in the form of strain energy, and transforms most of that strain energy into controlled displacements of its output points such that the given beam segment conforms to the specified final shape within a prescribed degree of accuracy.

For the design of the compliant mechanism, we assume that the bounds on weight or dimensions of the mechanism, a preferred region for the location of the input actuator, and an acceptable tolerance of error in the desired final shape are specified as design constraints. We measure the error in the final shape in terms of the least squares error (LSE) between the achieved displacements and the desired displacements at a sufficiently large number of points on the given beam segment. We also assume that the displacements of all points on the beam segment are small in order for the linear beam theory to be valid, and the segments of the structure are slender so that axial and shear strains are negligible.

Synthesis Procedure

The core design issue in the development of the approach described above is the synthesis of a compliant mechanism that correlates the desired continuous deformation of the given beam to a single input actuation, consistent with the task specifications and the design constraints. We divide the synthesis procedure into two subproblems: topological synthesis and dimensional synthesis.[35] In topological synthesis, we identify the points on the given beam segment that are optimal to connect the compliant mechanism, and from these points, we generate a satisfactory topology for the compliant mechanism. In dimensional synthesis we determine the dimensions of all segments of the mechanism, as well as the location and the magnitude of the input actuation. The various tasks in the synthesis procedure are illustrated schematically in Fig. 1 and explained in detail in the following sections.

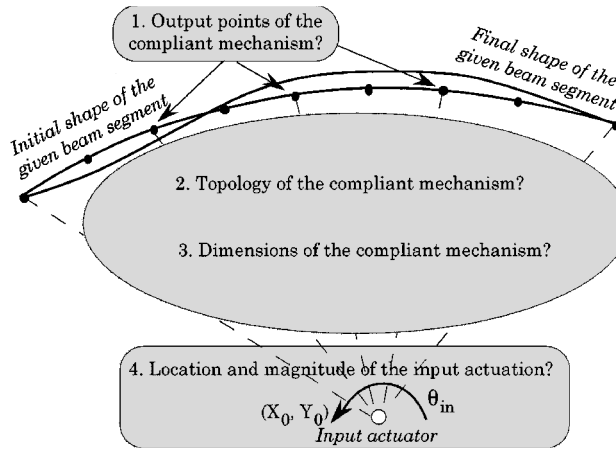

Fig. 1 Schematic representation of various tasks in the synthesis procedure.

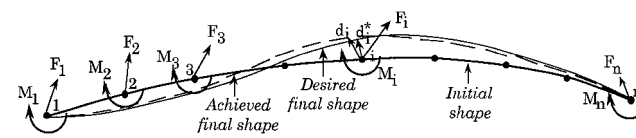

Fig. 2 Scheme to determine the optimal set of activation points on the beam segment.

Topological Synthesis

The topology, i.e., the structural form, of the compliant mechanism is influenced largely by two factors: the prescribed tolerance and the geometric complexity of the desired shape change. These two factors, in turn, are regulated by the number and the locations of the points where the compliant mechanism activates the given beam segment. Therefore, in this procedure, a set of optimal activation points on the given segment are determined first, and then the topology of the required compliant mechanism is sprouted from the identified points. In general, the larger the number of activation points, the better the accuracy of the achievable shape change will be, but at the same time, the larger the number of activation points, the more the number of segments in the topology and the heavier the weight of the system will be. Therefore, to satisfy the prescribed accuracy without encumbering the weight of the system, the minimum required number of activation points and their optimal locations on the beam segment are determined as follows.

At the outset, we identify along the length of the given beam segment a sufficiently large number of n points where the desired displacements are either explicitly specified or to be computed from the equation of the specified final shape (Fig. 2). These n points can be equally spaced but do not necessarily have to be so. Out of these n points, a subset of m points will be selected as the output points of the compliant mechanism. The minimum value of m and the optimal locations of the m activation points are determined through an iterative technique. This technique is initiated by setting m equal to a small value, say $m = 2$, and identifying the first m points in the sequence of the n points as the activation points. Then, the following algorithm is applied to compute the LSE of displacements at the n points as a result of activation of the current set of m points:

1) Assume n forces $F_i\,(i = 1 \ldots n)$ and n moments $M_i\,(i = 1 \ldots n)$ applied at each of the n points on the contour (see Fig. 2).

2) Obtain the reactions (forces and moments) at the two ends in terms of F_i and $M_i\,(i = 1 \ldots n)$ symbolically, using energy methods and the boundary-condition information.

3) Express the moment distribution along the contour, $M(s)$, as a function of F_i and $M_i\,(i = 1 \ldots n)$, and the arc length s of the contour. Compute the total strain energy associated with the shape change in terms of the assumed moments and forces (symbolically):

$$U = \frac{1}{2}\int \frac{M(s)}{EI}\,\mathrm{d}s$$

where E is the elastic modulus and I is the second moment of inertia of the cross section of the contour.

4) Compute the displacements at all of the n points due to forces at the m points using the energy method, and express the displacements only in terms of the active moments, $M_1, M_2, \ldots, M_m$, by setting all other forces and moments to be dummy forces and dummy moments:

$$d_i = \frac{\partial U}{\partial F_i}$$

where d_i is the displacement and F_i is the force at the ith point $(i = 1 \ldots n)$, respectively.

5) Compute the LSE:

$$e = \sum_{i=1}^{n} \frac{1}{2} w_i \left(d_i^* - d_i\right)^2$$

where d_i^* is the desired displacement at the ith point, d_i is the achieved displacement at the same point, and w_i is the associated weighting factor.

6) Minimize the error with respect to each of the active moments. Each minimization results in a linear equation in terms of the m active moments, $M_1, M_2, \ldots, M_m$:

$$\frac{\partial e}{\partial M_i} = 0 \Rightarrow E_i(M_1, M_2, \ldots, M_m) = 0$$

In all, this step results in m linear equations in m unknowns, viz. $M_1, M_2, \ldots, M_m$.

7) Solve the m linear equations in m unknowns; substitute the values obtained for the actuating moments $M_1, M_2, \ldots, M_m$ in the expression for the LSE e, in step 5, and compute the numerical value of e.

This algorithm is applied to each of all other possible combinations of selecting m points out of the total n points, and the LSE for each such combination of m points is computed. If the smallest value of the LSEs computed for the current value of m is within the prescribed tolerance of LSE, then the algorithm is stopped. Otherwise, the above algorithm is applied again for $m = m + 1$. This procedure is repeated until the LSE of displacements between the desired and the achieved shapes is smaller than the specified tolerance of LSE. The final value of m and the corresponding locations of those m points are selected as the output points of the compliant mechanism.

The next step in the synthesis is to generate the topology of the compliant mechanism, a framework of beam segments that connects the output points identified on the beam segment to the yet to be located input actuation point. The necessary basic framework comprises beam segments connecting the output points to the input point as shown in Fig. 3. However, such a topology lacks internal kinematic degrees of freedom (DOF) essential for a single-input/multi-output mechanism. Hence, to introduce internal DOF into the topology of the mechanism, the basic framework is augmented with additional cross segments to create a monolithic structure with internal nodes as shown in Fig. 4. Each internal node introduces three DOF. Although the exact coordinates of the nodes are dependent on the location of the input actuator to be determined later in the dimensional synthesis, the nodes are assumed to be located at points that are equally spaced along the lines joining the input and the output points. This topology is, of course, not unique but is rather simple to construct and provides a satisfactory solution.

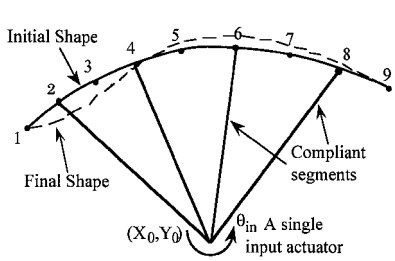

Fig. 3 Basic topology for compliant mechanism.

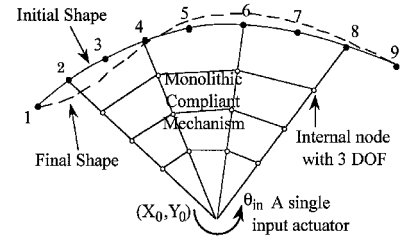

Fig. 4 Topology of the compliant mechanism including internal DOF.

Dimensional Synthesis

The suitable dimensions of all of the segments of the compliant mechanism as well as the specific location and the magnitude of the input actuation are determined next. All of these unknown quantities concurrently affect the relationship between the input actuation and the output displacements. Therefore, all of these unknowns are determined simultaneously by including them as design variables in a structural optimization scheme. The objective of the optimization is to minimize the LSE between two sets of displacements, one corresponding to the desired shape and the other corresponding to the achieved shape. The objective function may be weighted with appropriate weights w_i to influence the accuracy of a certain portion of the shape, if necessary. The constraints for the problem are the equilibrium equation of the structure expressed as $[\boldsymbol{K}]\{\boldsymbol{d}\} = \{\boldsymbol{F}\}$ through a standard finite element procedure, where $[\boldsymbol{K}]$ is the stiffness matrix and $\{\boldsymbol{d}\}$ and $\{\boldsymbol{F}\}$ are the displacement and force vectors, respectively; the upper bound on the total volume $V_{\max}$ of the mechanism; and the lower and upper bounds on the design variables, viz. the cross-sectional areas A_i of all segments of the mechanism, the location of the actuation point (X_0, Y_0), and the magnitude of the input rotation, θ_{in}. The optimization problem is posed as

Minimize:

$$\text{LSE} = e = \sum_{i=1}^{n} \frac{1}{2} w_i \left(d_i^* - d_i\right)^2$$

Subject to:

$$\text{Equilibrium: } [\boldsymbol{K}]\{\boldsymbol{d}\} = \{\boldsymbol{F}\}$$
$$\text{Volume} \le V_{\max}$$
$$A_{\min} \le A_i \le A_{\max}$$
$$\theta_{\min} \le \theta_{\text{in}} \le \theta_{\max}$$
$$(X_{\min}, Y_{\min}) \le (X_0, Y_0) \le (X_{\max}, Y_{\max})$$

The converged solution yields a set of values for all of the design variables, viz. A_i, θ_{in}, and (X_0, Y_0). With appropriate bounds on the design variables, and with sufficient number of DOF in the mechanism, this optimization routine usually converges to an LSE value that is lower than the value of LSE admitted in the topological synthesis. Therefore, the resulting shape should be within the prescribed accuracy.

Example: Static Shape Control of an Airfoil Camber

The synthesis procedure described above is generalized for shape control of any slender curved beam segment. The procedure can be extended to effect static shape changes at the leading and trailing edges of an airfoil by specially synthesized compliant mechanisms powered by only one actuator at each edge, as shown in the schematic in Fig. 5. The entire actuation system including the compliant mechanisms and the actuator can be located within the enclosure of the airfoil so that the external surface of the airfoil remains smooth. The compliant mechanisms effect the desired shape changes in the airfoil by transforming the input torque (or rotation) into controlled displacements of a finite number of discrete points on the airfoil contour. The input actuator could be any torque generating source (with adequate power for the task) such as a conventional electrical servomotor or a smart material-based torque tube. The initial and the desired final camber shapes are assumed to be specified along with an acceptable tolerance for the final shape. The procedure for

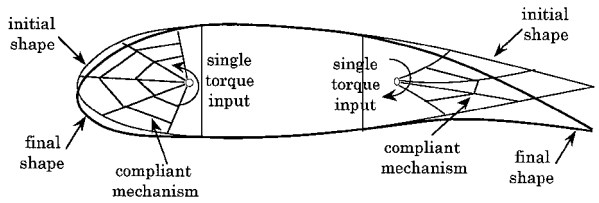

Fig. 5 Schematic of shape control of leading and trailing edges of an airfoil using compliant mechanisms.

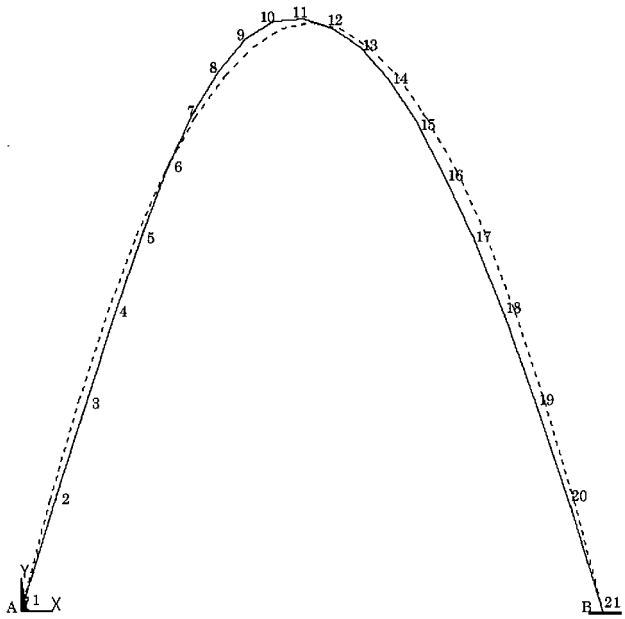

Fig. 6 Initial shape (– – –) and final shape (——) of the beam segment.

synthesis of a compliant mechanism for camber shaping of an airfoil is exemplified below through a simplified model of the leading edge represented as a curved beam segment without any loss of generality.

Consider a curved beam of uniform square section of 10×10 mm with its principal bending axis oriented along the curve (the dashed curve in the Fig. 6) given by the equation $y^2 = 400 - 0.01(x - 200)^2$ in an x-y Cartesian coordinate system. The two ends of the curve at points $A(x = 0)$ and $B(x = 400)$ are assumed to be fixed. This initial state of the beam is assumed to be stress-free with no external loading. Let the final desired shape (solid curve in Fig. 6) of the beam segment be specified through the x-component displacements of 19 points (equally spaced along the x axis) on the beam segment. These 19 points, plus the two end points, are labeled 1 through 21 in Fig. 6. Also, let the prescribed tolerance of error in the resulting final shape of the beam be an LSE of $\varepsilon^* = 1.0$ corresponding to the x-component displacements of the 19 points. The Young's modulus of the beam's material is assumed to be $E = 200 \times 10^3$ N/mm^2, although the topology of the compliant mechanism will be independent of the value of E.

Topological Synthesis

In this example, because the desired x-component displacements at 21 points on the contour are readily available, let $n = 21$, and let the desired displacements at the 21 points be denoted by d_i^*, $i = 1, \ldots, 21$. Let the reaction forces and moments at the fixed end A of the contour in Fig. 6 be denoted by $F_{A,x}$, $F_{A,y}$, M_A, where the first subscript denotes the location and the second subscript denotes the component of the force. Likewise, let the forces and moments at the 19 prescribed points be denoted by $F_{i,x}$, $F_{i,y}$, M_i, $i = 2, \ldots, 20$. The moment distribution of the contour is given by the symbolic equation

$$m_i(x) = F_{A,y}x - F_{A,x}y(x) - \sum_{i=2}^{n-1} F_{i,x}[y(x) - y(x_i)] - M_A - \sum_{2}^{i} M_i \tag{1}$$

where $m_i(x)$ is the moment distribution on the segment of the curve between the ith and $(i+1)$th points, and x_i is the x coordinate of the ith point, $i = 1, \ldots, 20$. This moment distribution expression can be simplified by eliminating the reactions $F_{A,x}$, $F_{A,y}$, M_A from Eq. (1). This is rendered by expressing the reactions in terms of the external forces and moments $F_{i,x}$, $F_{i,y}$, M_i using energy methods and the basic principles of statics.

First, by applying statics principles, $F_{A,y}$ is expressed in terms of $F_{i,x}$, $F_{i,y}$, M_i:

$$F_{A,y} = \frac{1}{L}\left\{M_A + M_B + \sum_{i=2}^{n-1}[M_i - F_{i,x}y(x_i)]\right\} \tag{2}$$

where L is the straight-line distance between the end points A and B, and M_B is the reaction moment at the end B. Then, plugging Eq. (2) into Eq. (1), and using the boundary-condition information (displacement at A, $d_{A,x} = 0$; rotation at A, $\theta_A = 0$; and rotation at B, $\theta_B = 0$), the reactions $F_{A,x}$, M_A, and M_B are expressed in terms of $F_{i,x}$, $F_{i,y}$, M_i by solving the equations

$$d_{A,x} = \sum_{i=1}^{n-1}\left[\int_{x_i}^{x_{i+1}} \frac{m_i(x)}{EI}\frac{\partial m_i(x)}{\partial F_{A,x}}\sqrt{1 + \frac{\mathrm{d}y(x)}{\mathrm{d}x}}\,\mathrm{d}x\right] = 0$$

$$\theta_A = \sum_{i=1}^{n-1}\left[\int_{x_i}^{x_{i+1}} \frac{m_i(x)}{EI}\frac{\partial m_i(x)}{\partial M_A}\sqrt{1 + \frac{\mathrm{d}y(x)}{\mathrm{d}x}}\,\mathrm{d}x\right] = 0 \tag{3}$$

$$\theta_B = \sum_{i=1}^{n-1}\left[\int_{x_i}^{x_{i+1}} \frac{m_i(x)}{EI}\frac{\partial m_i(x)}{\partial M_B}\sqrt{1 + \frac{\mathrm{d}y(x)}{\mathrm{d}x}}\,\mathrm{d}x\right] = 0$$

Then, using the resulting expressions of $F_{A,x}$, M_A, and M_B, the moment distribution is expressed as a function of only the applied symbolic loads and the x coordinate:

$$m_i(x) = f(F_{i,x}, F_{i,y}, M_i, x) \tag{4}$$

Next, a minimal number m of the n points and their optimal locations to be activated by the compliant mechanism are determined by applying the previously described algorithm as follows. Because the deformation is predominantly pure bending, the activations at the m points are considered to be pure moments. Accordingly, the external moments M_i at m ($<n$) activation points are considered active moments, and the external moments M_i at the rest $(19 - m)$ points as well as all the external forces, $F_{i,x}$ and $F_{i,y}$, at the 19 points are eventually made dummy loads during the computation of displacements. The minimum value of m and the optimal locations of the m activation points required to satisfy the prescribed accuracy for the shape change are determined through a combinatorial search technique. This search technique is begun by first setting m equal to a small value, e.g., 2 or 3, and then activating a set of m points at a time and computing the LSE between the resulting shape and the exact desired shape. Such errors are computed for all possible combinations of m points chosen out of the set of 19 points, and the combination that leads to the smallest LSE, ε_m, constitutes the best set of activation points for the current value of m. If $\varepsilon_m \le \varepsilon^*$, then the corresponding value of m and their locations are chosen as the optimal activation points. If $\varepsilon_m > \varepsilon^*$, then m is set to $m + 1$ and the new ε_m is computed. This procedure is repeated until $\varepsilon_m \le \varepsilon^*$. For instance, for $m = 2$, all possible combinations of two activation points, such as (2, 3), (2, 4), . . . , (19, 20), are considered, and the corresponding LSEs are computed. Of these, the LSE associated with the combination (4, 7), $\varepsilon_m = 10.67$, can be shown to be the smallest, and therefore 4 and 7 are the best activation points for $m = 2$. The details of the computation of ε_m corresponding to the activation points 4 and 7 are explained below.

The displacements at all 19 points, d_i, $i = 2, \ldots, 20$, are obtained in terms of M_4 and M_7 by applying the energy method to the general

expression of moment distribution in Eq. (4) treating all forces and moments except M_4 and M_7 as dummy loads:

$$d_{i,x} = \sum_{i=1}^{n-1} \left[\int_{x_i}^{x_{i+1}} \frac{m_i(x)}{EI} \frac{\partial m_i(x)}{\partial F_{i,x}} \sqrt{1 + \frac{\mathrm{d}y(x)}{\mathrm{d}x}}\, \mathrm{d}x \right] \tag{5}$$

The LSE ε_m between the desired displacements d_i^* and the achieved displacements $d_{i,x}$ is expressed as

$$\varepsilon_m = \sum_{i=2}^{20} w_i \left(d_{i,x}^* - d_{i,x}\right)^2 \tag{6}$$

where w_i is the weighting term associated with the ith point displacement. After the substitution for $d_{i,x}$ from Eq. (5) into Eq. (6), and equally weighting the displacements at all of the points, the resulting expression for ε_m can be simplified and expressed as

$$\varepsilon_m = 0.13598 \times 10^{-5} M_4^2 - 0.11616 \times 10^{-5} M_4 M_7 + 0.39425 \times 10^{-6} M_7^2 - 0.03601 M_4 + 0.001544 M_7 + 576.5796 \tag{7}$$

Differentiation of this expression for ε_m with respect to M_4 and M_7 leads to two equations that are linear in M_4 and M_7 as follows:

$$\begin{aligned} &\frac{\partial \varepsilon_m}{\partial M_4} = 0 \Rightarrow 0.271975 \times 10^{-5} M_4 \\ &\quad + 0.1161692 \times 10^{-5} M_7 + 0.036010 = 0 \\ &\frac{\partial \varepsilon_m}{\partial M_7} = 0 \Rightarrow -0.116169 \times 10^{-5} M_4 \\ &\quad + 0.788511 \times 10^{-6} M_7 + 0.001544 = 0 \end{aligned} \tag{8}$$

By solving these two linear equations, the values of M_4 and M_7 are obtained as

$$M_4 = 33458.88\ \text{N-mm}, \qquad M_7 = 47335.98\ \text{N-mm} \tag{9}$$

Substitution of these values of M_4 and M_7 in Eq. (7) results in $\varepsilon_m = 10.67$, the numerical value of LSE corresponding to the activation of points 4 and 7.

However, this value of $\varepsilon_m = 10.67$, the smallest of all LSEs corresponding to $m = 2$, is much higher than the acceptable value of $\varepsilon^* = 1.0$. This confirms that two activation points are not sufficient. Therefore, the number of activation points is increased to $m_{i+1} = m_i + 1 = 3$, and the above procedure is repeated. The smallest LSEs obtained for each of the values of $m = 2, 3, 4, 5$, and 6 are presented in Table 1.

It can be seen that a minimum of six points ($m = 6$) must be activated to achieve the specified shape change within the prescribed accuracy, and the best combination of points to activate is 2, 3, 9, 10, 19, and 20. Therefore, this set of six points on the contour is selected as output points of the mechanism.

Next, the topology of the compliant mechanism is generated in two stages. First, the basic framework of the topology (Fig. 7a) is created by connecting the six identified output points to the yet to be located input actuation point with beam segments. Then, it is augmented with additional beam segments to introduce an adequate number of design variables and internal kinematic DOF in the mechanism. As a rule of thumb, it was found that creating at least as many internal nodes in the mechanism as the number of points where constrained displacements are sought yields satisfactory results. Thus, accounting for the 19 constrained displacement points on the contour, 19 internal nodes are created in the mechanism by adding three layers of cross segments to the basic topology. This results in a topology with 39 segments in the compliant mechanism, as shown in Fig. 7b.

Table 1 Smallest LSEs corresponding to various sets of activation points

Number of activation points, m	Locations of set of m activated points that yields the smallest LSE, ε_m	Smallest LSE, ε_m, corresponding to the current value of m
2	4 and 7	10.69
3	5, 9, and 10	5.902
4	2, 8, 11, and 17	3.082
5	2, 9, 10, 19, and 20	1.068
6	2, 3, 9, 10, 19, and 20	0.818

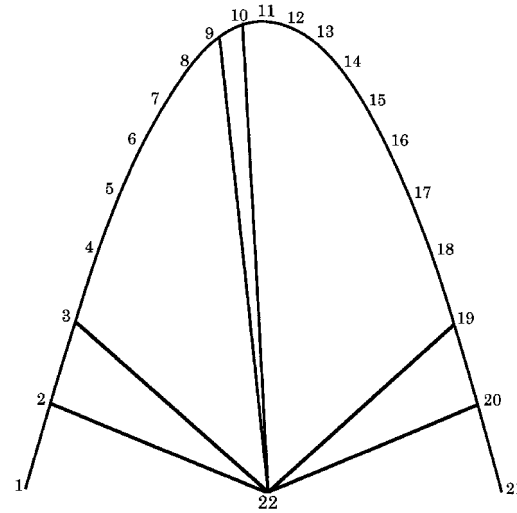

a) Basic topology

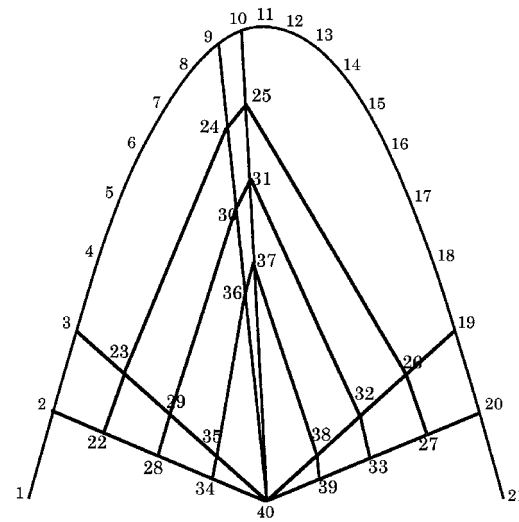

b) Topology with internal DOF

Fig. 7 Results of topological synthesis of compliant mechanism.

Dimensional Synthesis

In this example, we consider all of the segments of the compliant mechanism to be of constant 10 mm thick for the purpose of facilitating the fabrication of the system. The various unknown dimensions of the system include the widths b_i of the 39 segments of the mechanism, the location of the input actuator (X_0, Y_0), and the magnitude of the input actuation (rotation) θ_{in}. The optimal values of these unknowns are determined through an optimization scheme with the objective of minimizing the LSE of the x-component displacements of points 2 through 20 on the contour in the Fig. 7b. The equilibrium of the entire structure, i.e., the compliant mechanism along with the given beam segment, is expressed as $[\boldsymbol{K}]\{\boldsymbol{d}\} = \{\boldsymbol{F}\}$ using a finite element procedure and embedded in the optimization routine. Because it is desirable to locate the input actuator within the area enclosed by the contour of the given beam segment and the straight line connecting its two ends, we incorporate the bounds $(0, 0) \leq (X_0, Y_0) \leq (400, 300)$ as design constraints. The bounds on b_i and θ_{in} are chosen arbitrarily. The minimization problem is posed as follows:

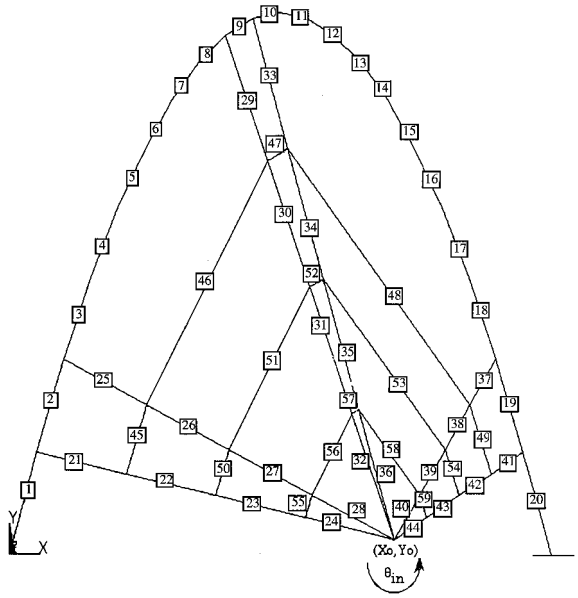

Converged value of the design variable	Converged value of the design variable
b_{21} = 2.8412 mm	b_{42} = 25.000 mm
b_{22} = 0.1158 mm	b_{43} = 25.000 mm
b_{23} = 25.000 mm	b_{44} = 25.000 mm
b_{24} = 21.960 mm	b_{45} = 23.801 mm
b_{25} = 4.1521 mm	b_{46} = 24.957 mm
b_{26} = 2.0500 mm	b_{47} = 1.6353 mm
b_{27} = 22.002 mm	b_{48} = 25.000 mm
b_{28} = 1.9266 mm	b_{49} = 9.4529 mm
b_{29} = 0.3924 mm	b_{50} = 19.969 mm
b_{30} = 0.1001 mm	b_{51} = 10.019 mm
b_{31} = 4.7138 mm	b_{52} = 3.8771 mm
b_{32} = 0.1000 mm	b_{53} = 25.000 mm
b_{33} = 1.5221 mm	b_{54} = 4.1592 mm
b_{34} = 25.000 mm	b_{55} = 20.637 mm
b_{35} = 25.000 mm	b_{56} = 0.1000 mm
b_{36} = 0.1000 mm	b_{57} = 8.4081 mm
b_{37} = 5.8536 mm	b_{58} = 17.221 mm
b_{38} = 25.000 mm	b_{59} = 0.1000 mm
b_{39} = 0.1242 mm	θ_{in} = 0.7000 rad.
b_{40} = 25.000 mm	X_0 = 284.80 mm
b_{41} = 25.000 mm	Y_0 = 10.241 mm

Fig. 8 Results of dimensional synthesis of compliant mechanism.

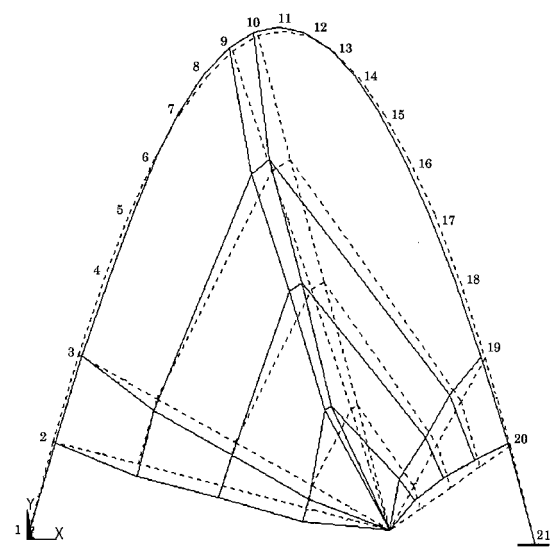

The point number	Desired displacement in mm.	Achieved displacement in mm.
2	3.1192	3.1395
3	4.7526	4.7122
4	4.9068	5.0488
5	3.1762	3.3578
6	0.6029	0.8544
7	–1.6632	–1.6001
8	–3.6660	–3.5005
9	–5.3441	–4.6618
10	–5.3380	–5.0967
11	–5.0123	–5.0843
12	–5.3154	–5.1994
13	–6.0676	–5.7177
14	–7.0095	–6.6347
15	–7.9029	–7.6869
16	–8.5046	–8.4089
17	–8.3416	–8.3089
18	–7.3306	–7.1890
19	–5.4964	–5.6188
20	–2.9724	–2.9796

Fig. 9 Verification of results through finite element analysis.

Minimize:

$$\text{LSE}, \varepsilon = \sum_{i=2}^{20} \left(d^*_{i,x} - d_{i,x}\right)^2$$

Subject to:

$$\text{Equilibrium:} [\boldsymbol{K}]\{\boldsymbol{d}\} = \{\boldsymbol{F}\}$$
$$0.1\,\text{mm} \le b_i \le 25\,\text{mm} \quad \forall\, i = 21, \ldots, 59$$
$$-0.7\,\text{rad} \le \theta_{\text{in}} \le 0.7\,\text{rad}$$
$$(0, 0) \le (X_0, Y_0) \le (400, 300)$$

This problem is solved using the optimization toolbox in the MATLAB™ program starting with initial guesses $b_i = 10\,\text{mm}$, $\theta_{\text{in}} = 0.5$ rad, and $(X_0, Y_0) = (200, 0\,\text{mm})$. The optimization converged to an LSE $\varepsilon = 0.4$. The converged values of b_i (widths of segments numbered 21 through 59), θ_{in}, and (X_0, Y_0) are shown in Fig. 8. To confirm the results, a finite-element analysis was conducted on the structure in Fig. 8 with the optimized dimensions. The results of the analysis are shown in Fig. 9, where the diagram on the left shows the initial and the final states of the structure in dashed and solid lines, respectively, and the table on the right compares the achieved displacements with the desired displacements at the 19 specified points on the given beam segment. It can be seen from the table in Fig. 9 that the achieved shape compares well with the desired shape.

Conclusions

A novel approach is introduced to effectuate desired shape changes in generally curved beam segments using compliant mechanisms, and a generalized procedure is developed for systematic synthesis of such mechanisms. The synthesis procedure is illustrated through an example of camber shaping of an idealized airfoil. The highlight of the proposed approach is that it operates on a rather simple system comprising only an elastic structural frame and a single input actuator. The input actuator can be any torque generating device including a conventional electric servomotor, and as such, this approach is not affected by the stroke limitation of smart materials as in the embedded actuation schemes. Moreover, this approach significantly simplifies the necessary control system by reducing the number of input actuators to just one. Additionally, because the actuator in this approach can be located away from the structure, the actuators and the mechanism can be protected from undesirable effects such as exposure to unstructured environment and stress concentrations as in the case of embedded actuation schemes. This is especially useful in the camber shaping of wing structures where

it is desirable to enclose the actuation system completely within the contour of the airfoil, leaving the external surface smooth for a drag-free performance. Further, by virtue of compliant mechanisms, this approach is inherently friction-free and backlash-free. The only shortcoming in this approach is that achievable shape changes are approximations of the exact desired shape changes; however, the accuracy of the approximations can be monitored by appropriately choosing the design constraints in the optimization. In conclusion, the results indicate that this approach is viable for real-scale practical applications without some of the limitations of the other approaches. However, more comprehensive experimental studies on dynamically scaled models are required to validate the proposed approach before it can be extended to real-scale applications such as the adaptive VCW.

Acknowledgment

The authors gratefully acknowledge the support provided for this research by the U.S. Air Force Office of Scientific Research under Grant F49620-96-1-0205.

References

[1]Spillman, W. B., Jr., Sirkis, J. S., and Gardiner, P. T., "Smart Materials and Structures: What Are They?" *Smart Materials and Structures*, Vol. 5, No. 3, 1996, pp. 247–254.

[2]Kashiwase, T., Tabata, M., Tsuchiya, K., and Akishita, S., "Shape Control of Flexible Structures," *Journal of Intelligent Material Systems and Structures*, Vol. 2, No. 1, 1991, pp. 110–125.

[3]Balas, M. J., "Optimal Quasi-Static Shape Control for Large Aerospace Antennae," *Journal of Optimization Theory and Applications*, Vol. 46, No. 2, 1985, pp. 153–170.

[4]Austin, F., Rossi, M. J., Nostrand, W. V., Knowles, G., and Jameson, A., "Static Shape Control for Adaptive Wings," *AIAA Journal*, Vol. 32, No. 9, 1994, pp. 1895–1901.

[5]Noor, A. K., Venneri, S. L., Paul, D. B., and Chang, J., "New Structures for New Aerospace Systems," *Aerospace America*, Vol. 35, No. 11, 1997, pp. 26–31.

[6]Sobieczky, H., Fung, K. Y., and Seebass, A. R., "A New Method for Designing Shock-Free Transonic Configurations," AIAA Paper 78-1114, July 1978.

[7]Chacksfield, J. E., "Variable Camber Airfoils," *Aeronautical Journal*, Vol. 84, No. 832, 1980, pp. 131–139.

[8]Gilbert, W. W., "Mission Adaptive Wing System for Tactical Aircraft," *Journal of Aircraft*, Vol. 18, No. 7, 1981, pp. 597–602.

[9]Spillman, J. J., "The Use of Variable Camber to Reduce Drag, Weight and Costs of Transport Aircraft," *Aeronautical Journal*, Vol. 96, No. 951, 1992, pp. 1–9.

[10]Szodruch, J., "The Influence of Camber Variation on the Aerodynamics of Civil Transport Aircraft," AIAA Paper 85-0353, Jan. 1985.

[11]Renken, J. H., "Mission Adaptive Wing Camber Control Systems for Transport Aircraft," AIAA Paper 85-5006, Oct. 1985.

[12]Redeker, G., Wichmann, G., and Oelker, H.-C., "Aerodynamic Investigations Toward an Adaptive Airfoil for Transonic Transport Aircraft," *Journal of Aircraft*, Vol. 23, No. 5, 1986, pp. 398–405.

[13]Greff, E., "The Development and Design Integration of a Variable Camber Wing for Long/Medium Range Aircraft," *Aeronautical Journal*, Vol. 94, No. 939, 1990, pp. 301–312.

[14]Fielding, J. P., and Vaziry-Zanjany, M. A. F., "Reliability, Maintainability and Development Cost Implications of Variable Camber Wings," *Aeronautical Journal*, Vol. 100, No. 995, 1996, pp. 183–195.

[15]Scott, W. B., "Performance Gains Confirmed in Mission Adaptive Wing Tests," *Aviation Week and Space Technology*, Vol. 129, No. 77, 1988, p. 77.

[16]Kudva, J. N., Appa, K., Van, C. B., and Lockyer, A. J., "Adaptive Smart Wing Design for Military Aircraft: Requirements, Concepts, and Payoffs," *Proceedings of the SPIE Smart Structures and Materials 1995: Industrial and Commercial Applications of Smart Structures Technologies*, edited by C. R. Crowe and G. L. Anderson, Vol. 2447, International Society for Optical Engineering, Bellingham, WA, 1995, pp. 35–44.

[17]Chaudhry, Z., and Rogers, C. A., "Bending and Shape Control of Beams Using SMA Actuators," *Journal of Intelligent Material Systems and Structures*, Vol. 2, No. 4, 1991, pp. 581–602.

[18]Beauchamp, C. H., Nadolink, R. H., Dickinson, S. C., and Dean, L. M., "Shape Memory Alloy Adjustable Camber (SMACC) Control Surfaces," *Proceedings of the First European Conference on Smart Structures and Materials*, edited by B. Culshaw, P. T. Gardiner, and A. McDonach, SPIE Vol. 1777, Inst. of Physics and European Optical Society/International Society for Optical Engineering, Bristol, England, UK, 1992, pp. 189–192.

[19]Maclean, B. J., Carpenter, B. F., Draper, J. L., and Misra, M. S., "A Compliant Wing Section for Adaptive Wing Surfaces," *Proceedings of the ADPA/AIAA/ASME/SPIE Conference on Active Materials and Adaptive Structures*, edited by G. Knowles, Inst. of Physics, Bristol, England, UK, 1992, pp. 281–284.

[20]Austin, F., Siclari, M. J., Van Nostrand, W., Weisensel, G. N., Kottamasu, V., and Volpe, G., "Comparison of Smart Wing Concept for Transonic Cruise Drag Reduction," *Proceedings of the SPIE Smart Structures and Materials 1997: Industrial and Commercial Applications of Smart Structures Technologies*, edited by J. M. Sater, Vol. 3044, International Society for Optical Engineering, Bellingham, WA, 1997, pp. 33–40.

[21]Kudva, J. N., Appa, K., Jardine, A. P., Martin, C. A., and Carpenter, B. F., "Overview of Recent Progress on the DARPA/USAF Wright Laboratory Smart Materials and Structures Development—Smart Wing Program," *Proceedings of the SPIE Smart Structures and Materials 1997: Industrial and Commercial Applications of Smart Structures Technologies*, edited by J. M. Sater, Vol. 3044, International Society for Optical Engineering, Bellingham, WA, 1997, pp. 24–32.

[22]Ehlers, S. M., and Weisshaar, T. A., "Static Aeroelastic Control of an Adaptive Lifting Surface," *Journal of Aircraft*, Vol. 30, No. 4, 1993, pp. 534–540.

[23]Lazarus, K. B., Crawley, E., and Bohlmann, J. D., "Static Aeroelastic Control Using Strain Actuated Adaptive Structures," *Journal of Intelligent Material Systems and Structures*, Vol. 2, No. 3, 1991, pp. 386–410.

[24]Midha, A., "Elastic Mechanisms," *Modern Kinematics—The Developments in the Last Forty Years*, edited by A. G. Erdman, Wiley, New York, 1993, Chap. 9.

[25]Ananthasuresh, G. K., and Saggere, L., "One Piece Compliant Stapler," Dept. of Mechanical Engineering and Applied Mechanics, Univ. of Michigan, Rept. TR UM-MEAM 95-20, Ann Arbor, MI, July 1995.

[26]Smith, S. T., and Chetwynd, D. G., *Foundations of Ultraprecision Machine Design*, Gordon and Breach, Montreaux, Switzerland, 1992, Chap. 4.

[27]Ananthasuresh, G. K., Kota, S., and Gianchandani, Y., "A Methodical Approach to the Synthesis of Compliant Micromechanisms," *Technical Digest*, Solid-State Sensor and Actuator Workshop (Hilton Head, SC), Transducers Research Foundation, Cleveland Heights, OH, 1994, pp. 189–192.

[28]Saggere, L., Kota, S., and Crary, S. B., "A New Design for Suspension of Linear Microactuators," *Proceedings of the 1994 International Mechanical Engineering Congress and Exposition: Dynamic Systems and Control*, edited by C. J. Radcliffe, Vol. ASME DSC 55-2, American Society of Mechanical Engineers, New York, 1994, pp. 671–675.

[29]Paros, J. M., and Weisbord, L., "How to Design Flexure Hinges," *Machine Design*, Vol. 37, No. 27, 1965, pp. 151–156.

[30]Burns, R. H., "The Kinetostatic Synthesis of Flexible Link Mechanisms," Ph.D. Dissertation, Mechanical Engineering Dept., Yale Univ., New Haven, CT, 1964.

[31]Sevak, N. M., and McLarnan, C. W., "Optimal Synthesis of Flexible Link Mechanisms with Large Static Deflections," *Journal of Engineering for Industry*, Vol. 97, Series B, No. 2, 1975, pp. 520–526.

[32]Howell, L. L., and Midha, A., "A Method for the Design of Compliant Mechanisms with Small-Length Flexural Pivots," *Journal of Mechanical Design*, Vol. 116, No. 1, 1994, pp. 280–290.

[33]Frecker, M. I., Ananthasuresh, G. K., Nishiwaki, S., Kikuchi, N., and Kota, S., "Topological Synthesis of Compliant Mechanisms Using Multi-Criteria Optimization," *Journal of Mechanical Design*, Vol. 119, No. 2, 1997, pp. 238–245.

[34]Sigmund, O., "On the Design of Compliant Mechanisms Using Topology Optimization," *Mechanics of Structures and Machines*, Vol. 25, No. 4, 1997, pp. 493–524.

[35]Saggere, L., "Static Shape Control of Smart Structures: A New Approach Utilizing Compliant Mechanisms," Ph.D. Dissertation, Dept. of Mechanical Engineering and Applied Mechanics, Univ. of Michigan, Ann Arbor, MI, 1998.

A. Chattopadhyay
Associate Editor